Cerebral Cortex, November 2015;25: 4628–4637

doi: 10.1093/cercor/bhv121
Advance Access Publication Date: 5 June 2015
Original Article

ORIGINAL ARTICLE

A Diffusion MRI Tractography Connectome of the Mouse Brain and Comparison with Neuronal Tracer Data

Evan Calabrese, Alexandra Badea, Gary Cofer, Yi Qi, and G. Allan Johnson

Center for In Vivo Microscopy, Duke University Medical Center, Department of Radiology, Duke University Medical Center, Durham, NC 27710, USA

Address correspondence to Dr G. Allan Johnson, Center for In Vivo Microscopy, Box 3302 Duke University Medical Center, Durham, NC 27710, USA. Email: gjohnson@duke.edu

Abstract

Interest in structural brain connectivity has grown with the understanding that abnormal neural connections may play a role in neurologic and psychiatric diseases. Small animal connectivity mapping techniques are particularly important for identifying aberrant connectivity in disease models. Diffusion magnetic resonance imaging tractography can provide nondestructive, 3D, brain-wide connectivity maps, but has historically been limited by low spatial resolution, low signal-to-noise ratio, and the difficulty in estimating multiple fiber orientations within a single image voxel. Small animal diffusion tractography can be substantially improved through the combination of ex vivo MRI with exogenous contrast agents, advanced diffusion acquisition and reconstruction techniques, and probabilistic fiber tracking. Here, we present a comprehensive, probabilistic tractography connectome of the mouse brain at microscopic resolution, and a comparison of these data with a neuronal tracer-based connectivity data from the Allen Brain Atlas. This work serves as a reference database for future tractography studies in the mouse brain, and demonstrates the fundamental differences between tractography and neuronal tracer data.

Key words: connectome, magnetic resonance imaging, mouse, neuroanatomy, tractography

Introduction

Brain connectivity mapping has emerged as a major focus of neuroscience research, in part due to the recognition that altered neural connectivity may contribute to a number of neurologic and psychiatric diseases (Konrad and Eickhoff 2010; Lo et al. 2010; Skudlarski et al. 2010; Xue et al. 2014). Several techniques have been used to explore structural brain connectivity in animal models including anterograde/retrograde tracer studies (Swanson 1982; Oh et al. 2014), two-photon tomography (Ragan et al. 2012), diffusion magnetic resonance imaging (MRI) tractography (Mori et al. 1999), and polarized light imaging (Larsen et al. 2007; Axer et al. 2011). Neuronal tracer studies have become the de facto gold standard for brain connectivity mapping because of their high sensitivity and specificity; however, these studies are limited by the requirement for stereotaxic tracer injections, 2D (slice) imaging, and the inability to study multiple pathways within a single brain.

Diffusion MRI tractography—the 3D tracing of water diffusion pathways measured by MRI—offers a noninvasive method for brain connectivity mapping. Tractography is generated from anatomically defined seed regions of arbitrary size (above image resolution), shape, and number, allowing a complete connectivity map, or connectome, to be developed from a single brain. Despite these benefits, diffusion tractography has historically been limited to the study of gross connectivity between distant anatomic regions, and generally fails to accurately represent mesoscale brain connectivity (i.e., ~100 µm resolution) (Oh et al. 2014). This limitation is primarily due to the low spatial resolution and low signal-to-noise ratio (SNR) of diffusion MRI, and

the difficulty in resolving subvoxel fiber complexity (Fillard et al. 2011).

Three distinct technologies have emerged that can dramatically increase the sensitivity of diffusion tractography for detecting mesoscale brain connectivity: 1) imaging of fixed ex vivo specimens treated with MRI contrast agents allows considerably higher spatial resolution, higher SNR, and longer acquisition times than would be possible with in vivo imaging (Johnson et al. 2012; Lerch et al. 2012); 2) advanced diffusion acquisition and processing techniques like Q-ball (Tuch 2004), spherical deconvolution (Tournier et al. 2004), and diffusion spectrum imaging (Wedeen et al. 2008) provide accurate modeling of multiple fiber populations within a single image voxel; and 3) probabilistic tractography techniques yield increased sensitivity for detecting nondominant fiber pathways (Behrens et al. 2007). The combination of these 3 techniques represents a novel method for exploring brain connectivity in postmortem brain specimens from virtually any species, although it is currently most practical in small animal models due to imaging hardware and scan time requirements.

Neuronal connections in the mouse brain have been investigated more thoroughly than in virtually any other mammalian species. The Allen Brain Atlas (ABA) mouse brain connectome is one of the most comprehensive attempts to map mouse brain connectivity, and includes data from nearly 500 unique anterograde viral neuronal tracer injections in the wild-type C57BL/6 mouse brain (Oh et al. 2014). These data provide a unique opportunity to explore the similarities and differences between microscopic diffusion tractography and neuronal tracer data in the mouse brain.

Here, we present the first comprehensive diffusion tractography connectome of the mouse brain at microscopic resolution, and a brain-wide comparison of tractography data with neuronal tracer data from the ABA. The tractography-based connectome has several advantages over neuronal tracer-based connectomes; 1) all pathways are derived from a single brain instead of different brains for each pathway; 2) tractography seed regions are based on anatomy rather than stereotaxic tracer injections; and 3) the data are 3D, and interactive, so users can explore the connectivity of arbitrarily defined seed regions at will. However, tractography-based connectivity data are fundamentally different from neuronal tracer-based data, and suffers from several limitations that complicate its interpretation. For example, tractography is based on water diffusion orientation, which is an imperfect surrogate for underlying axonal orientation, and is incapable of distinguishing anterograde versus retrograde connections. To explore these differences and limitations, we compare microscopic probabilistic tractography data with neuronal tracer data from all 488 wild-type tracer injection sites available through the ABA using 3D colocalization and connectivity-based analyses. The data presented here can serve as a reference database for future tractography studies of the mouse brain and as a test of the fundamental limits of the diffusion tractography technique.

Materials and Methods

Specimen Preparation

Animal experiments and procedures were carried out in compliance with the Duke University Institutional Animal Care and Use Committee. Two wild-type adult male C57BL/6 mice weighing approximately 27 g were chosen for imaging. The animals were perfusion-fixed and doped with gadolinium contrast agent using the active staining technique described more thoroughly elsewhere (Johnson et al. 2012). In short, the animals were transcardially perfused with a solution of 10% neutral buffered formalin and 50 mM gadoteridol (ProHance, Bracco Diagnostics). Immediately prior to imaging, the brain specimens, still intact inside the neurocranium, were placed in a custom-made MRI compatible tube and immersed in liquid fluorocarbon (Galden PFPE, Solvay Plastics).

Diffusion MRI

Imaging was performed on a 9.4-Tesla small animal imaging system controlled by an Agilent VnmrJ 4 console. A custom-made silver solenoid coil was used for radiofrequency transmission and reception. Diffusion imaging was accomplished using a 3D diffusion-weighted spin-echo pulse sequence with repetition time (TR) = 100 ms, echo time (TE) = 15 ms, and b-value = 4000 s/mm^2. The acquisition matrix was $568 \times 284 \times 228$ over a 24.4 mm × 12.2 mm × 9.8 mm field of view, resulting in a native isotropic image resolution of 43 µm. The diffusion sampling protocol included 120 unique diffusion directions (Koay 2011; Koay et al. 2011) and 11 nondiffusion-weighted (b0) measurements (i.e., one b0 every 12 diffusion measurements). Total acquisition time was 235 h. Bore temperature was controlled with a chilled water pump and monitored with a fiber-optic probe for the duration of the experiment (Supplementary Fig. 1).

Data Processing

Data processing was done on a high-performance computing cluster with 96 physical cores and 1.5 TB of RAM. After image reconstruction, all 131 image volumes were registered to the first b0 image using Advanced Normalization Tools (ANTs) affine transformation (Avants et al. 2011) to correct for the linear portion of eddy current distortions. Scalar image volumes were reconstructed using FSL's DTIFIT-weighted least-squares tensor estimation (Behrens et al. 2003). Fiber data for probabilistic tractography were reconstructed using FSL's BEDPOSTX (Behrens et al. 2007) with a maximum of 4 fiber orientations per voxel.

Anatomic Segmentation

Image data were acquired with the brain inside the skull to preserve native spatial relationships. A brain tissue mask was generated using a previously described automated skull-stripping algorithm (Badea et al. 2007) based on interactive thresholding and binary morphological operations. Automated atlas-based anatomic segmentation was performed as previously described (Sharief et al. 2008) using 2 different reference label sets: the Waxholm Space atlas of the mouse brain (Johnson et al. 2010) for subcortical labels, and the Ullmann et al. atlas of the mouse neocortex (Ullmann et al. 2013) for cortical labels. After automated image segmentation, the resulting labels were manually corrected to ensure anatomic accuracy. Labels were split along the midline to generate separate label sets for the left and right hemispheres of the brain.

Probabilistic Tractography

Probabilistic tractography was performed using FSL's PROBTRACKX (Behrens et al. 2007). Tracking parameters included 5000 samples per voxel, a step size of 21 µm, and a curvature threshold of 45°. Probabilistic tractography maps were individually generated for the left and right halves of each of the 148 anatomic labels (i.e., 296 total tractography datasets per specimen).

For waypoint connectivity studies, one or more label masks were used as target regions, and only fibers passing through these targets were included in output maps.

Connectivity Analysis

All 296 seed region tractography maps from each specimen were used to generate tractography-based connectivity estimates. For a given seed region A, the corresponding tractography dataset represents all connections from region A to the rest of the brain. To estimate connectivity from region A to another region B, all fibers from A that fall within B were summed, regardless of path or termination point. Connectivity estimates were then normalized by the volume of the seed region to correct for differences in the total number of tractography seeds per structure. Connectivity estimates were used to populate a 296 × 296 weighted, directed, connectivity matrix. Connectivity matrix data are available for download in multiple formats at http://www.civm.duhs.duke.edu/mouseconnectome/.

Comparison with Allen Brain Atlas Neuronal Tracer data

To assess similarities and differences between tractography and neuronal tracer data, we performed 3D colocalization and connectivity-based comparisons of microscopic diffusion tractography data with ABA neuronal tracer data. A separate set of tractography maps was generated from the 488 wild-type tracer injection sites included in the ABA connectome. First, diffusion MRI datasets were registered to the ABA mouse brain atlas image using ANTs automated image registration. Tracer injection sites were modeled as spherical regions of interest (ROIs) centered at the injection coordinates provided by the ABA, with volume equal to the tracer injection volume. Injection site ROIs were then transformed back to the native space of the diffusion MRI data and used to generate probabilistic tractography maps. Finally, tractography maps were transformed into ABA space for direct comparison with tracer data.

Colocalization analysis was used to assess the 3D overlap between spatially normalized probabilistic tractography images and ABA neuronal tracer projection energy images. Projection energy is defined as the product of density (number of pixels with tracer signal) and intensity (total tracer signal per pixel). 3D projection energy data were downloaded in from the ABA website (http://connectivity.brain-map.org/) in MetaImage format, and converted to NIfTI format for further analysis. Both tractography and projection energy data were log-transformed and normalized between zero and one. Colocalization was assessed as voxel-wise Spearman rank correlation between the 2 image volumes within a whole-brain mask. Nonparametric correlation was used because we did not assume a linear relationship between tracer projection energy and probabilistic tractography fiber count.

Injection site ROI tractography data were also used for connectivity-based comparisons with ABA tracer data. Tractography-based connectivity estimates between injection site ROIs and targets from the ABA mouse brain anatomic segmentation were generated using the previously described methods. A 469 injection site ROI by 592 anatomic region (296 on each side of the brain) weighted, directed, connectivity matrix was generated, corresponding to the tracer-based connectivity matrix provided by the ABA (Oh et al. 2014). Connectivity data were log-transformed, normalized between zero and one, and compared

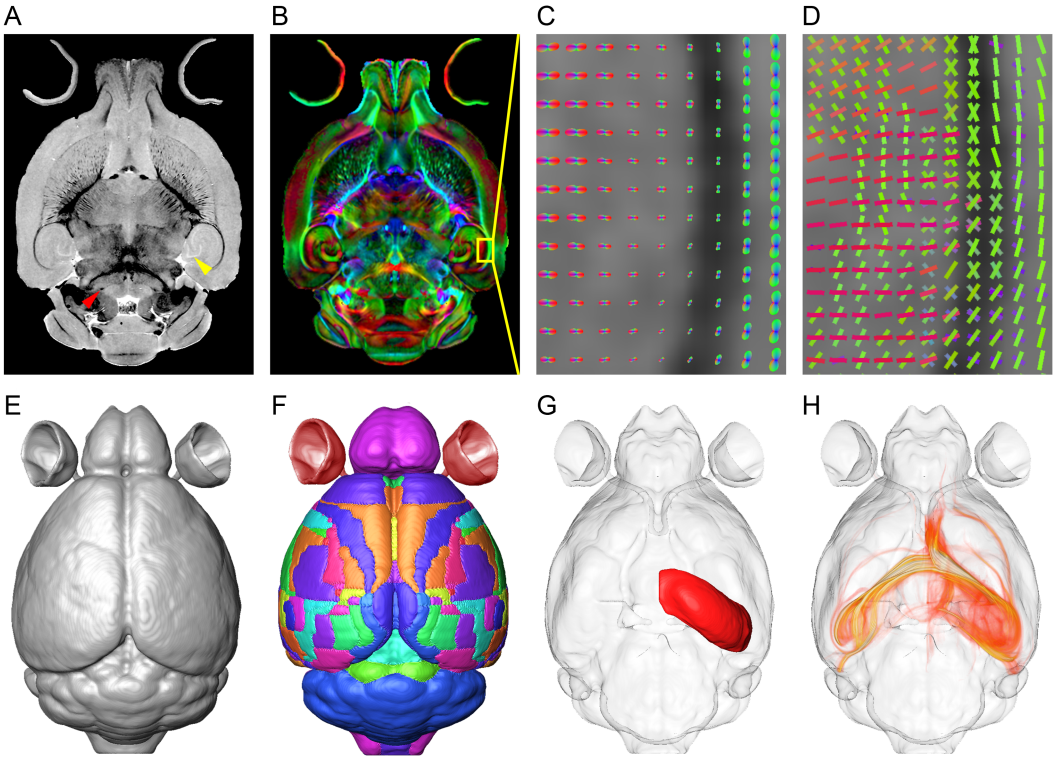

Figure 1. A schematic of the tractography data-processing pipeline. (*A*) Representative anatomic image. Arrows indicate the mesencephalic trigeminal tract (red) and granule cell layer of the dentate gyrus (yellow). (*B*) Representative diffusion data (color fractional anisotropy). (*C*) A magnified view of the ventrolateral hippocampus shows estimates of the diffusion orientation distribution function at each voxel. (*D*) Multiple fiber orientations estimated from diffusion data. (*E*) Automatically generated brain mask. (*F*) Automated atlas-based segmentation of 148 distinct anatomic structures. (*G*) The seed region for the right hippocampal formation. (*H*) Volume-rendered probabilistic tractography data for the seed region shown in (*G*).

using Spearman rank correlation at 3 different levels of detail. First, the complete 469 × 592 connectivity matrices were compared directly (seed-level comparison). Connectivity matrices were then binarized using a series of thresholds that preserved 10–100% of connections. The resulting binary connectivity matrices were compared using receiver operatic characteristic (ROC) analysis with tracer-based connectivity as ground truth. To assess similarity on a mid-level scale, total connectivity from all seed ROIs/injection sites to a given anatomic structure were summed (structure-level comparison). Finally, for the coarsest-scale analysis, anatomic regions were collapsed (summed) into their parent structures according to the ABA ontology (parent-level comparison).

Interexperiment Diffusion Tractography Differences

All tractography-based connectivity experiments were repeated on a second mouse brain specimen. The resulting connectivity matrix was compared with both the ABA neuronal tracer-based connectivity matrix and to the first tractography-based connectivity matrix using the methods described in the previous section. For tractography to tractography connectivity matrix comparisons, ROC analysis was replaced by simple percent agreement and percent disagreement since ground truth is not currently defined for tractography.

Results

Probabilistic Tractography Mapping of the Whole Mouse Brain

The diffusion MRI data used for this study are, to our knowledge, the highest spatial resolution diffusion MRI data ever reported for the whole mouse brain. At an isotropic voxel size of 43 µm, the spatial resolution is approximately 30 000 times higher

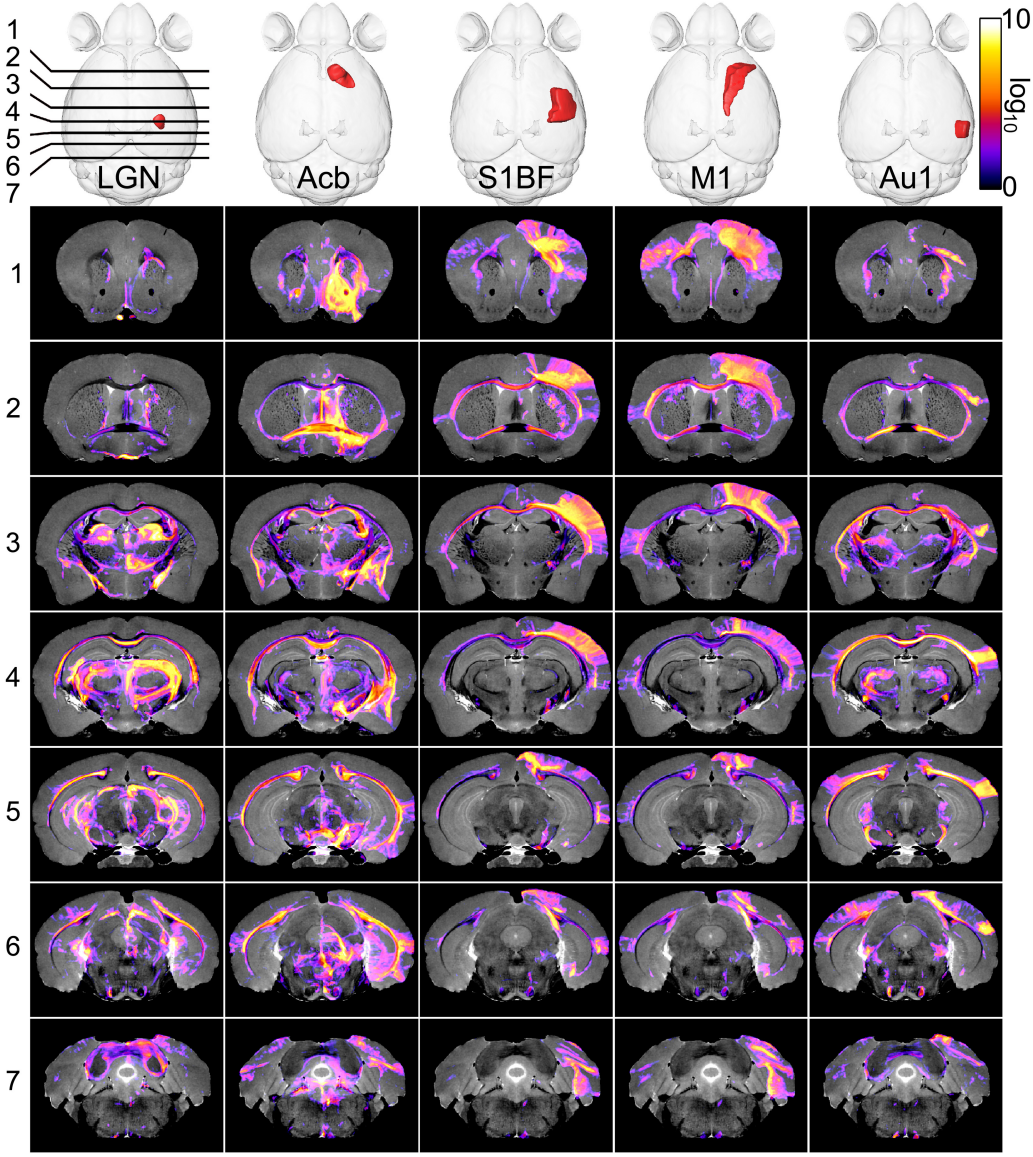

Figure 2. Representative seed region connectivity maps displayed as color overlays on standard anatomic MR images. The seed region is displayed in red along the top row within a transparent surface rendering of the brain. Seven different coronal slices are shown for each connectivity map, as indicated by the slice diagram in the top left corner. Connectivity data are displayed with a $\log_{10}$ scale color map (top right). LGN, lateral geniculate nucleus; Acb, accumbens nucleus; S1BF, primary somatosensory cortex barrel field; M1, primary motor cortex; Au1, primary auditory cortex.

resolution than a typical human diffusion MRI scan, and 10 times higher after accounting for the approximately 3000-fold difference in total brain volume (Herculano-Houzel 2009). At this resolution, many microscopic features, including cell layers and small white matter tracts, can be identified (Fig. 1A,B, arrows). The final dataset consists of approximately 6.5 million in-brain voxels, and 121 distinct diffusion measurements per voxel, for a total data volume of nearly 800 million points. Each diffusion measurement is a discrete sample of the diffusion probability distribution function within a voxel (Fig. 1C) from which the underlying fiber orientation(s) are estimated (Fig. 1D). Multiple fiber orientations per voxel are possible, if supported by the data, up to a maximum of four. In these data, over 72% of brain voxels were found to have 2 or more fiber populations (Supplementary Fig. 2), suggesting that accounting for multiple fiber populations is essential, even at high spatial resolution.

After initial diffusion data processing, probabilistic tractography connectivity maps were systematically generated for 148 different anatomic regions in each hemisphere of the mouse brain (296 total). First, automated skull-stripping was used to segment brain tissue from surrounding muscle and connective tissue. The resulting brain mask (Fig. 1E) includes the optic nerves and retinae, which are embryologic derivatives of the ventral forebrain and thus considered to be part of the brain. The skull-stripped brain image data were automatically segmented using 148 reference labels (Fig. 1F) and manually edited to ensure anatomic accuracy. The label set was divided along the midline to produce separate labels for each hemisphere, which were then used as seed regions for probabilistic tractography (Fig. 1G,H).

Individual connectivity maps were generated for each seed region (i.e., 296 connectivity maps total, 148 for each hemisphere). These seed region connectivity maps represent all connections from a given region to the rest of the brain. The value of a given voxel is the total number of tracks originating from the seed region that pass through or terminate in that voxel, which is used as a surrogate for relative connection probability. The absolute connectivity value depends on the number of voxels in the seed region and the number of times each voxel is seeded for tractography. We observed a connection probability range of 10^{10} across the entire dataset after normalizing for the total number of voxels in each seed region. Five representative seed region connectivity maps are presented as color overlays on top of standard anatomic MR images (Fig. 2). These same seed region connectivity maps can be visualized as 3D volume renderings (Supplementary Fig. 3). Probabilistic tractography was able to reproduce a majority of connections that have been previously shown with other methods including corticospinal motor pathways (Fig. 2; M1, rows 1–7) and interhemispheric connections

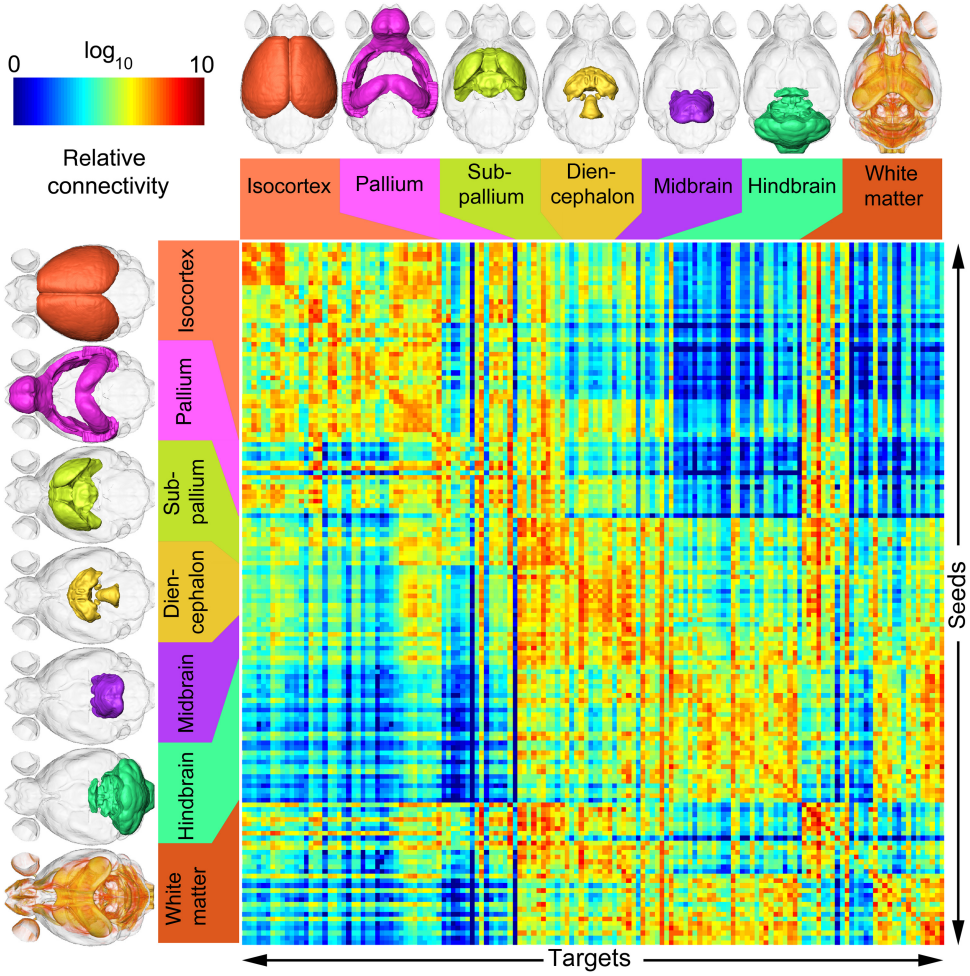

Figure 3. A probabilistic tractography connectivity matrix for the mouse brain. Relative connectivity estimates between 148 anatomic regions are displayed with a $\log_{10}$ scale color map (top left). Tractography seeds (rows) and targets (columns) are organized based on their developmental origins as indicated by colored surface renderings of parent structures along the top and left side of the figure. The complete structure list is presented in order in Supplementary Table 1.

between the primary auditory cortices (Fig. 2; Au1, row 5). Many tractography maps also included connections that have not been previously observed (e.g., callosal connections from the lateral geniculate nucleus), which could be attributed to false positives, or to the fundamental differences between connectivity mapping techniques. Complete connectivity maps for all 296 seed regions are available online for visualization and download at http://www.civm.duhs.duke.edu/mouseconnectome/.

Connectivity Matrix Analysis

Probabilistic tractography data were used to generate brain-wide connectivity matrices. To facilitate visualization, seed regions were organized into groups based on their embryologic origins as outlined by the Puelles et al. (2013) developmental ontology of the mouse brain. The complete hierarchical organization for the 148 anatomic structures used in this study is presented in Supplementary Table 1. One notable deviation from the Puelles et al. ontology is the inclusion of a separate parent group for white matter structures. This was done because many white matter pathways span multiple embryologically distinct anatomic regions (Fig. 3).

Connectivity estimates were generated for all 296 seed region tractography datasets and all 296 anatomic regions. Importantly, because seeding was done independently for each region, the connectivity estimate between seed region A and target region B is not necessarily the same as that between seed region B and target region A. As a result, 4 different connectivity matrices were generated—right seeds to right targets, right seeds to left targets, left seeds to right targets, and left seeds to left targets (Supplementary Fig. 4). The average of all 4 connectivity matrices reflects bilateral connectivity (Fig. 2). In general, ipsilateral connectivity was higher than contralateral connectivity, which is consistent with previous studies of the mouse brain (Oh et al. 2014). Right and left connectivity maps showed strong mirror image similarity, suggesting a high degree of lateral symmetry in mouse brain connections. Small lateral asymmetries were observed in the anterior pallium, prepontine hindbrain, and forebrain white matter tracts (Supplementary Fig. 5). Although there is evidence for laterally asymmetric connectivity in the human brain (Toga and Thompson 2003), the extent to which these asymmetries are conserved in mice is unknown.

Waypoint Connectivity Mapping

One feature that distinguishes diffusion MRI tractography from other brain connectivity mapping techniques is the ability to map only the pathways that connect 2 different regions. To accomplish this, tractography is generated at random from a seed region, and only those tracks that pass through a given target region (waypoint) are retained. This allows visualization of the specific pathway connecting 2 regions without extraneous connectivity to other regions. For example, we generated probabilistic tractography connecting the basolateral amygdaloid nucleus (BLA) to the ipsilateral cingulate cortex area 32 (A32, sometimes referred to as the prelimbic cortex) (Fig. 4). This pathway is believed to be involved in a variety of psychiatric diseases including schizophrenia and depression (Rosenkranz and Grace 2002). Probabilistic tractography shows connections coursing from the BLA, through the ventral striatum, then medially and dorsally toward the dorsal cingulate cortex (Fig. 4; right). These results are consistent with previous tractography experiments in the mouse (Gutman et al. 2012), and with neuronal tracer studies in the mouse and rat (Vertes 2004; Oh et al. 2014). The 3D nature of diffusion tractography

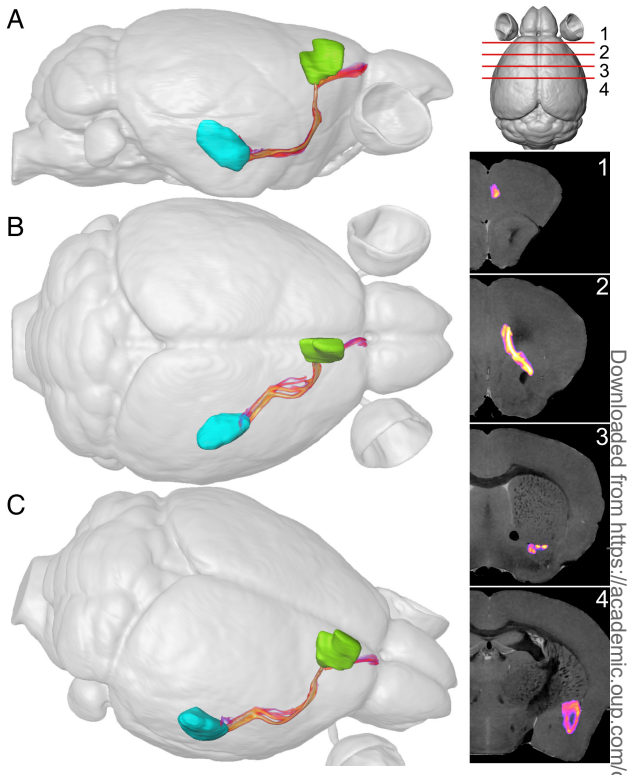

Figure 4. Waypoint connectivity map between the basolateral amygdaloid nucleus (BLA) and cingulate cortex area 32 (A32). (A–C) Three-dimensional renderings of the pathway are displayed within a transparent surface rendering of the brain from lateral (A), dorsal (B), and oblique (C) perspectives. Surface renderings of the BLA (blue) and A32 (green) are included for reference. Data are also displayed as color overlays on 4 coronal slices (right) as indicated by the slice diagram (top right). The color map used for overlays is the same as in Figure 2.

data allows this pathway to be visualized and manipulated in 3D as a volume-rendered object (Fig. 4A–C). Without the constraints of a waypoint, the pathway of interest is obscured by multiple other pathways emanating from the BLA (Supplementary Fig. 6).

Waypoint connectivity mapping can also employ more than one target region, further increasing the specificity of the resulting connectivity maps. For example, waypoint connectivity mapping of the superior colliculus with the lateral geniculate nucleus and contralateral retina as waypoints yields only the retinotectal portion of the visual pathway (Supplementary Fig. 7). Once again, these tractography results closely resemble results from other connectivity mapping methods (Linden and Perry 1983; Pautler et al. 1998). Different combinations of seed regions and waypoint regions yield a virtually infinite number of possible connectivity maps that can be generated from these data.

Comparison with the ABA Mouse Connectome

A separate set of tractography experiments was used to allow direct comparison with neuronal tracer data from the ABA. Probabilistic tractography data were generated from ROIs corresponding to each of the 488 wild-type neuronal tracer injection sites included in the ABA mouse connectivity atlas (Fig. 5A). These data were used for 3D colocalization and connectivity-based comparisons with corresponding ABA neuronal tracer datasets.

Colocalization analysis for both tractography datasets (i.e., 488 comparisons × 2) revealed weak but significant correlation between neuronal tracer data and probabilistic tractography (Fig. 5A,B). In total, 966/976 (99%) of correlations reached statistical

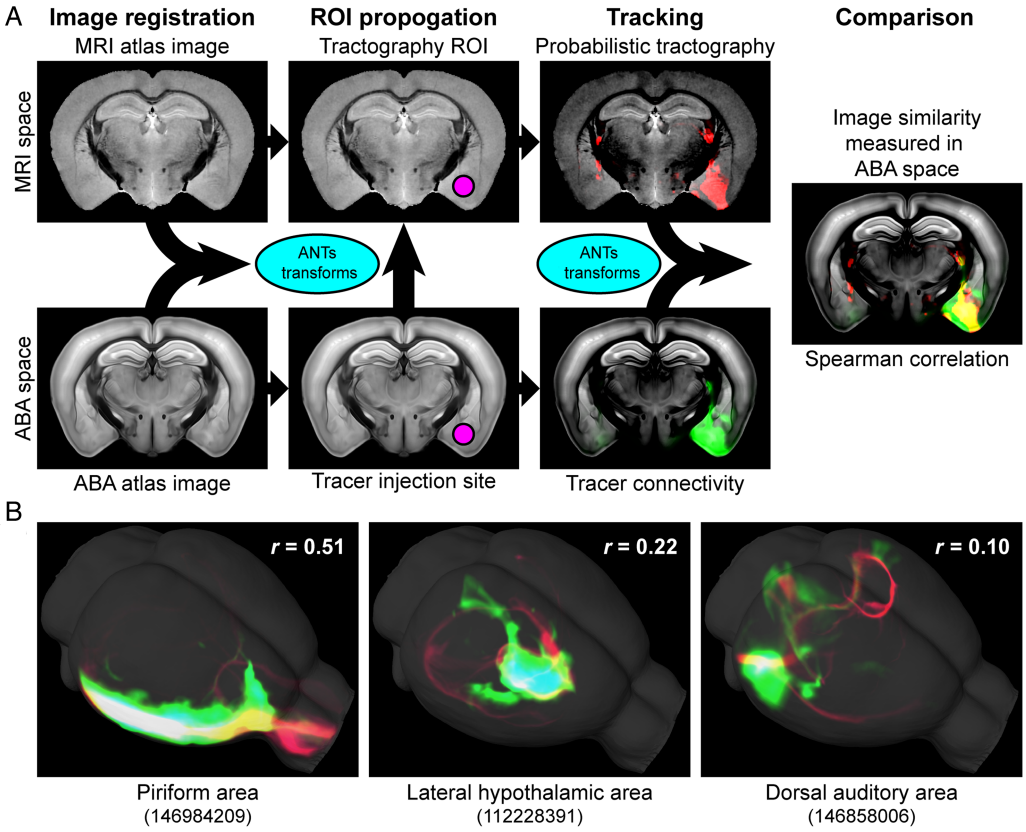

Figure 5. Colocalization analysis of spatially normalized tractography and ABA neuronal tracer data. (*A*) Schematic of the processing steps used to generate tractography data corresponding to the 488 wild-type mouse brain tracer injection experiments provided by the ABA. MRI images were registered to the ABA atlas image, and the resulting transforms were used to propagate ROIs modeling tracer injection sites into MRI space. Injection site ROIs were used to generate tractography data, which was compared directly with tracer data. (*B*) 3D colocalization of data from 3 representative sites. Tractography is shown in red, and ABA projection energy in green. Correlation values and injection site/ROI names and ABA ID numbers are included for each image.

significance, with 957/976 (98%) surviving Bonferroni correction for multiple comparisons. The average Spearman *r*-value was $r = 0.23 \pm 0.11$ with a range from $r = -0.06$ to 0.51 (Fig. 5*B*). Only 11/976 (1%) comparisons yielded negative correlation values. The average seed volume for comparisons with nonsignificant *P*-values and negative *r*-values was 0.03 and 0.16 mL, respectively, while the average seed volume for all comparisons was 0.25 mL. Tractography and neuronal tracer colocalization for all 488 injection sites/seed regions can be visualized interactively in 3D at http://www.duhs.duke.edu/mouseconnectome/.

Colocalization analysis measures the 3D overlap of pathways, but does not assess structural connectivity directly. The ABA provides a weighted, directed, connectivity matrix between 469 tracer injection sites and 296 anatomic regions on either side of the mouse brain (i.e., 592 total regions). An analogous tractography-based connectivity matrix was generated using tractography data generated from the 469 ROIs corresponding to the injection sites used for the ABA matrix (Fig. 6*A*). Tractography- and tracer-based connectivity matrices were compared at 3 levels of anatomic detail. Correlation at the finest, seed-to-target level was $r = 0.42$ ($P << 0.05$). The accuracy of tractography-based connectivity estimates at the finest level was further assessed using ROC analysis with tracer-based connectivity as the ground truth (Fig. 6*B*). Tractography yielded a true-positive rate of 61% and a false-positive rate of 26%. For the mid-level (structure-level) connectivity comparison, where all connections to a given target structure were summed, the correlation between tractography and tracer-based connectivity increased to $r = 0.71$ ($P << 0.05$) (Fig. 6*C*). Finally, for the coarsest, parent-level comparison, where all connections to each anatomic parent structure were summed, correlation increased to near unity ($r = 0.99$, $P << 0.05$) (Fig. 6*D*). Relative to neuronal tracer data, tractography tended to underestimate connectivity in the cortex, and overestimate connectivity in the midbrain and diencephalon (Fig. 6*C*,*D*). Graph data are available at http://www.duhs.duke.edu/mouseconnectome/.

Interexperiment Diffusion Tractography Differences

Connectivity matrices generated from 2 different mouse brain diffusion acquisitions were compared with each other to assess inter-study similarity (Supplementary Fig. 8). Correlation of weighted connectivity matrices revealed an *r*-value of $r = 0.81$ ($P << 0.05$), indicating a relatively strong relationship. With optimal thresholding, the 2 tractography studies had 87.5% agreement (12.5% disagreement).

Discussion

A growing body of evidence suggests that altered brain connectivity is present in a variety of neurologic and psychiatric diseases, yet identifying affected pathways in animal models remains difficult with conventional techniques. Neuronal tracer studies, while significantly more specific than tractography, are labor intensive, require an a priori hypothesis of the affected pathway, and are not amenable to studying multiple pathways within the same brain. Neuronal tracer-based connectomes, like the ABA mouse connectome, require the sacrifice of hundreds of animals,

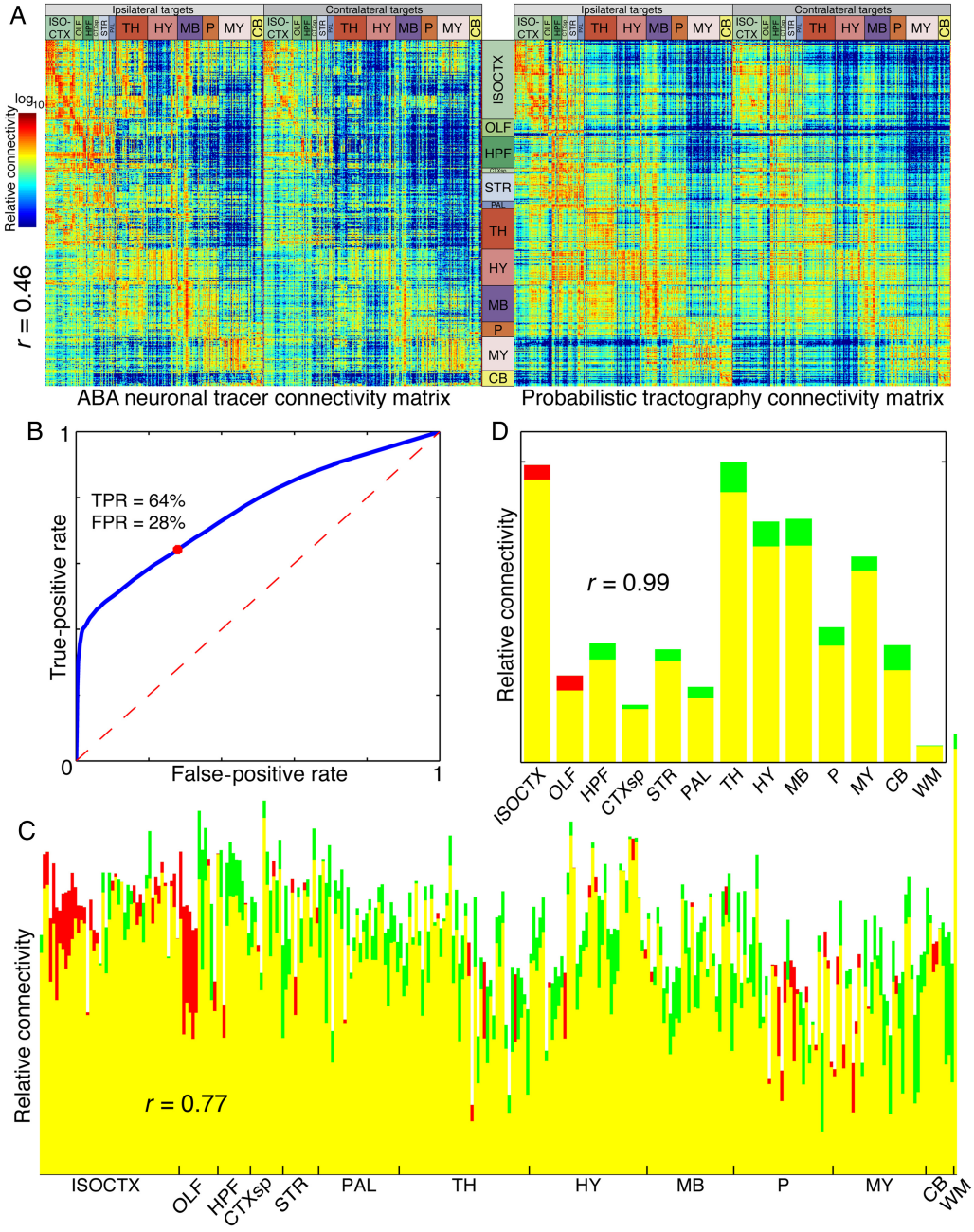

Figure 6. Connectivity-based analysis of tractography and ABA neuronal tracer data. (*A*) A 469 injection site ROI by 592 anatomic region connectivity matrices generated from ABA tracer data (left) and probabilistic tractography data (right). Matrix correlation (seed-level) was $r = 0.46$. (*B*) ROC analysis of tractography accuracy with ABA tracer data as ground truth. (*C*) Mid-level (structure-level) comparison of tractography-based connectivity with tracer-based connectivity. Tractography-based connectivity estimates are shown in red, tracer-based estimates in green, and overlap between the two in yellow. (*D*) Coarse (parent-level) comparison similar to (*C*) but collapsed into ontologically defined parent structures. Parent structure abbreviations are consistent with the ABA.

thousands of hours of imaging, and all of the associated monetary expenses. For these reasons, it is currently impractical to use neuronal tracer studies to screen for aberrant connectivity. In contrast, high-quality diffusion tractography data, have several features that are well suited to use as a survey tool: 1) they offer sensitive, whole-brain coverage within a single animal; 2) they are 3D, and thus do not require 3D reformatting; 3) data analysis is easily automated, including anatomic segmentation, fiber tracking, and connectivity estimation; and 4) the entire process is nondestructive to the tissue, thus allowing virtually any ex vivo brain imaging technique to be performed on the same tissue after MRI acquisition. False-positive results, though generally not an issue for survey tests, can be reduced to some extent with post hoc waypoint connectivity mapping. Once a potentially affected pathway is identified, results can be subsequently validated in the same specimen using more specific, destructive brain imaging techniques like conventional histology (Calabrese, Du et al. 2014) or electron microscopy (Calabrese and Johnson 2013).

Despite its many benefits, diffusion MRI of fixed ex vivo specimens also presents several unique challenges. Formalin fixation causes an approximately 4-fold reduction in brain diffusivity, thus requiring 4-fold higher *b*-value for in vivo equivalent

diffusion weighting. Fortunately, brain tissue diffusivity reduction appears to be uniform and proportional, thus preserving diffusion anisotropy and the ability to estimate fiber orientations from diffusion MRI of fixed specimens (Sun et al. 2005; Dyrby et al. 2011). Gadolinium doping does not affect diffusion MRI directly, but, in conjunction with fixation, causes dramatic reductions in tissue T1 and T2 relaxation times, which must be accounted for with careful pulse sequence design.

The data presented here required over 1 week for acquisition; however, the total time required to generate a brain-wide tractography connectivity map is comparable with the time required for a single neuronal tracer study, and could be reduced even further with faster MRI acquisition techniques and/or improved computational power. For example, we chose a relatively simple Cartesian diffusion spin-echo pulse sequence with <10% data-acquisition time efficiency (readout time/TR). A more time-efficient echo-planar or spiral pulse sequence could substantially reduce total scan time at the expense of a potential increase in image artifacts. In addition, multispecimen parallel imaging techniques could dramatically reduce acquisition time for group studies (Dazai et al. 2011). There is also considerable debate over the number of diffusion measurements necessary for multifiber estimation methods (Tournier et al. 2013; Calabrese, Badea et al. 2014). The values chosen for this study (120 diffusion measurements at $b = 4000$ s/mm^2) meet or exceed recommendations for optimal ex vivo diffusion imaging (Dyrby et al. 2011; Tournier et al. 2013), so it is reasonable to assume that similar results could be generated from a more sparsely sampled, and therefore faster to acquire dataset. Conversely, these results could potentially be improved with increased diffusion sampling at multiple b-values, particularly, when coupled with advanced diffusion sampling and reconstruction schemes like diffusion spectrum imaging (Wedeen et al. 2008) or generalized q-sampling imaging (Yeh et al. 2010).

Despite the high quality of the diffusion tractography data presented here, we observed relatively poor correspondence with neuronal tracer data, particularly with regard to 3D colocalization analysis. Connectivity results were slightly more similar; however, strong correlation results were only observed in the coarsest, parent structure-level connectivity analysis. Previous comparisons of tractography and tracer data have yielded similar results (Thomas et al. 2014). This is perhaps not surprising since tractography and neuronal tracer studies are fundamentally different. Anterograde viral tracers, like those used for the ABA mouse connectome, are unidirectional, follow individual axons, and do not cross synapses. In contrast, tractography is bidirectional, follows bundles of axons, and is not necessarily constrained by synapses. Connections present in tractography but absent in anterograde tracer data are presumed to be false positives, but could also represent true retrograde connections or true multisynaptic connections. Further, the fact that tractography is dissimilar from neuronal tracer data does not preclude its use as a method for structural brain mapping or detecting neuropathology. However, the biological interpretation of results remains the single greatest challenge to the diffusion tractography community, and further study, particularly in animal models where a gold standard for neuronal connectivity exists, will be essential for addressing this challenge.

As researchers continue to explore the role of brain connectivity in human health and disease, mouse models will undoubtedly remain a primary system for new discoveries, and new tools will be needed to identify subtle connectivity variations. The small animal diffusion tractography techniques presented here can provide brain-wide connectivity maps at microscopic image resolution and may prove useful in identifying aberrant connectivity in models of neurologic and psychiatric diseases. High-quality mouse tractography datasets, like those presented here, will be essential for understanding the neural basis of tractography, through direct comparisons with more specific, invasive connectivity methods like neuronal tracer studies and electrophysiology.

As is frequently the case, new research methods are not unambiguously superior to previous methods but rather provide new, different, and often complementary information. Diffusion MRI tractography is unlikely to supplant other small animal connectivity mapping techniques, but it does provide a nondestructive method for 3D, brain-wide connectivity mapping. Small animal diffusion tractography has already been used to identify specific connectivity-related pathology in a variety of disease models (Moldrich et al. 2010; Kerbler et al. 2012; Harsan et al. 2013), and the brain-wide connectivity assessment methods described here should serve to accelerate such findings. With attention to proper interpretation of results, and validation, diffusion tractography should continue to be a valuable tool for discovering new connectivity alterations in small animal models of human brain diseases.

Supplementary Material

Supplementary material can be found at: http://www.cercor.oxfordjournals.org.

Funding

This work was supported by 2 National Institutes of Health grants, the National Institute of Biomedical Imaging and Bioengineering (grant number P41 EB015897) and the National Institute on Aging (grant number K01 AG041211) to A.B. Funding to pay the Open Access publication charges for this article was provided by a grant from NIH/NIBIB (P41 EB015897).

Notes

Conflict of Interest: None declared.

References

Avants BB, Tustison NJ, Song G, Cook PA, Klein A, Gee JC. 2011. A reproducible evaluation of ANTs similarity metric performance in brain image registration. Neuroimage. 54:2033–2044.

Axer M, Grässel D, Kleiner M, Dammers J, Dickscheid T, Reckfort J, Hütz T, Eiben B, Pietrzyk U, Zilles K, et al. 2011. High-resolution fiber tract reconstruction in the human brain by means of three-dimensional polarized light imaging. Front Neuroinform. 5:34.

Badea A, Ali-Sharief AA, Johnson GA. 2007. Morphometric analysis of the C57BL/6J mouse brain. Neuroimage. 37:683–693.

Behrens TEJ, Berg HJ, Jbabdi S, Rushworth MFS, Woolrich MW. 2007. Probabilistic diffusion tractography with multiple fibre orientations: what can we gain? Neuroimage. 34:144–155.

Behrens TEJ, Woolrich MW, Jenkinson M, Johansen-Berg H, Nunes RG, Clare S, Matthews PM, Brady JM, Smith SM. 2003. Characterization and propagation of uncertainty in diffusion-weighted MR imaging. Magn Reson Med. 50:1077–1088.

Calabrese E, Badea A, Coe CL, Lubach GR, Styner MA, Johnson GA. 2014. Investigating the tradeoffs between spatial resolution and diffusion sampling for brain mapping with diffusion tractography: time well spent? Hum Brain Mapp. 35:5667–5685.

Calabrese E, Du F, Garman RH, Johnson GA, Riccio C, Tong LC, Long JB. 2014. Diffusion tensor imaging reveals white matter

injury in a rat model of repetitive blast-induced traumatic brain injury. J Neurotrauma. 31:938–950.

Calabrese E, Johnson GA. 2013. Diffusion tensor magnetic resonance histology reveals microstructural changes in the developing rat brain. Neuroimage. 79:329–339.

Dazai J, Spring S, Cahill LS, Henkelman RM. 2011. Multiple-mouse neuroanatomical magnetic resonance imaging. J Vis Exp. (48): pii: 2497.

Dyrby TB, Baaré WFC, Alexander DC, Jelsing J, Garde E, Søgaard LV. 2011. An ex vivo imaging pipeline for producing high-quality and high-resolution diffusion-weighted imaging datasets. Hum Brain Mapp. 32:544–563.

Fillard P, Descoteaux M, Goh A, Gouttard S, Jeurissen B, Malcolm J, Ramirez-Manzanares A, Reisert M, Sakaie K, Tensaouti F, et al. 2011. Quantitative evaluation of 10 tractography algorithms on a realistic diffusion MR phantom. Neuroimage. 56:220–234.

Gutman DA, Keifer OP, Magnuson ME, Choi DC, Majeed W, Keilholz S, Ressler KJ. 2012. A DTI tractography analysis of infralimbic and prelimbic connectivity in the mouse using high-throughput MRI. Neuroimage. 63:800–811.

Harsan L-A, Dávid C, Reisert M, Schnell S, Hennig J, von Elverfeldt D, Staiger JF. 2013. Mapping remodeling of thalamocortical projections in the living reeler mouse brain by diffusion tractography. Proc Natl Acad Sci USA. 110:E1797–E1806.

Herculano-Houzel S. 2009. The human brain in numbers: a linearly scaled-up primate brain. Front Hum Neurosci. 3:31.

Johnson GA, Badea A, Brandenburg J, Cofer G, Fubara B, Liu S, Nissanov J. 2010. Waxholm space: an image-based reference for coordinating mouse brain research. Neuroimage. 53:365–372.

Johnson GA, Calabrese E, Badea A, Paxinos G, Watson C. 2012. A multidimensional magnetic resonance histology atlas of the Wistar rat brain. Neuroimage. 62:1848–1856.

Kerbler GM, Hamlin AS, Pannek K, Kurniawan ND, Keller MD, Rose SE, Coulson EJ. 2012. Diffusion-weighted magnetic resonance imaging detection of basal forebrain cholinergic degeneration in a mouse model. Neuroimage. 66C:133–141.

Koay CG. 2011. A simple scheme for generating nearly uniform distribution of antipodally symmetric points on the unit sphere. J Comput Sci. 2:377–381.

Koay CG, Hurley SA, Meyerand ME. 2011. Extremely efficient and deterministic approach to generating optimal ordering of diffusion MRI measurements. Med Phys. 38:4795–4801.

Konrad K, Eickhoff SB. 2010. Is the ADHD brain wired differently? A review on structural and functional connectivity in attention deficit hyperactivity disorder. Hum Brain Mapp. 31:904–916.

Larsen L, Griffin LD, Grässel D, Witte OW, Axer H. 2007. Polarized light imaging of white matter architecture. Microsc Res Tech. 70:851–863.

Lerch JP, Gazdzinski L, Germann J, Sled JG, Henkelman RM, Nieman BJ. 2012. Wanted dead or alive? The tradeoff between in-vivo versus ex-vivo MR brain imaging in the mouse. Front Neuroinform. 6:6.

Linden R, Perry VH. 1983. Massive retinotectal projection in rats. Brain Res. 272:145–149.

Lo C-Y, Wang P-N, Chou K-H, Wang J, He Y, Lin C-P. 2010. Diffusion tensor tractography reveals abnormal topological organization in structural cortical networks in Alzheimer's disease. J Neurosci. 30:16876–16885.

Moldrich RX, Pannek K, Hoch R, Rubenstein JL, Kurniawan ND, Richards LJ. 2010. Comparative mouse brain tractography of diffusion magnetic resonance imaging. Neuroimage. 51:1027–1036.

Mori S, Crain BJ, Chacko VP, van Zijl PC. 1999. Three-dimensional tracking of axonal projections in the brain by magnetic resonance imaging. Ann Neurol. 45:265–269.

Oh SW, Harris JA, Ng L, Winslow B, Cain N, Mihalas S, Wang Q, Lau C, Kuan L, Henry AM, et al. 2014. A mesoscale connectome of the mouse brain. Nature. 508:207–214.

Pautler RG, Silva AC, Koretsky AP. 1998. In vivo neuronal tract tracing using manganese-enhanced magnetic resonance imaging. Magn Reson Med. 40:740–748.

Puelles L, Harrison M, Paxinos G, Watson C. 2013. A developmental ontology for the mammalian brain based on the prosomeric model. Trends Neurosci. 36:570–578.

Ragan T, Kadiri LR, Venkataraju KU, Bahlmann K, Sutin J, Taranda J, Arganda-Carreras I, Kim Y, Seung HS, Osten P. 2012. Serial two-photon tomography for automated ex vivo mouse brain imaging. Nat Methods. 9:255–258.

Rosenkranz JA, Grace AA. 2002. Cellular mechanisms of infralimbic and prelimbic prefrontal cortical inhibition and dopaminergic modulation of basolateral amygdala neurons in vivo. J Neurosci. 22:324–337.

Sharief AA, Badea A, Dale AM, Johnson GA. 2008. Automated segmentation of the actively stained mouse brain using multispectral MR microscopy. Neuroimage. 39:136–145.

Skudlarski P, Jagannathan K, Anderson K, Stevens MC, Calhoun VD, Skudlarska BA, Pearlson G. 2010. Brain connectivity is not only lower but different in schizophrenia: a combined anatomical and functional approach. Biol Psychiatry. 68:61–69.

Sun S-W, Neil JJ, Liang H-F, He YY, Schmidt RE, Hsu CY, Song S-K. 2005. Formalin fixation alters water diffusion coefficient magnitude but not anisotropy in infarcted brain. Magn Reson Med. 53:1447–1451.

Swanson LW. 1982. The projections of the ventral tegmental area and adjacent regions: a combined fluorescent retrograde tracer and immunofluorescence study in the rat. Brain Res Bull. 9:321–353.

Thomas C, Ye FQ, Irfanoglu MO, Modi P, Saleem KS, Leopold DA, Pierpaoli C. 2014. Anatomical accuracy of brain connections derived from diffusion MRI tractography is inherently limited. Proc Natl Acad Sci USA. 111:16574–16579.

Toga AW, Thompson PM. 2003. Mapping brain asymmetry. Nat Rev Neurosci. 4:37–48.

Tournier J-D, Calamante F, Connelly A. 2013. Determination of the appropriate b value and number of gradient directions for high-angular-resolution diffusion-weighted imaging. NMR Biomed. 26:1775–1786.

Tournier J-D, Calamante F, Gadian DG, Connelly A. 2004. Direct estimation of the fiber orientation density function from diffusion-weighted MRI data using spherical deconvolution. Neuroimage. 23:1176–1185.

Tuch DS. 2004. Q-ball imaging. Magn Reson Med. 52: 1358–1372.

Ullmann JFP, Watson C, Janke AL, Kurniawan ND, Reutens DC. 2013. A segmentation protocol and MRI atlas of the C57BL/6J mouse neocortex. Neuroimage. 78:196–203.

Vertes RP. 2004. Differential projections of the infralimbic and prelimbic cortex in the rat. Synapse. 51:32–58.

Wedeen VJ, Wang RP, Schmahmann JD, Benner T, Tseng WYI, Dai G, Pandya DN, Hagmann P, D'Arceuil H, de Crespigny AJ. 2008. Diffusion spectrum magnetic resonance imaging (DSI) tractography of crossing fibers. Neuroimage. 41:1267–1277.

Xue K, Luo C, Zhang D, Yang T, Li J, Gong D, Chen L, Medina YI, Gotman J, Zhou D, et al. 2014. Diffusion tensor tractography reveals disrupted structural connectivity in childhood absence epilepsy. Epilepsy Res. 108:125–138.

Yeh F-C, Wedeen VJ, Tseng W-YI. 2010. Generalized q-sampling imaging. IEEE Trans Med Imaging. 29:1626–1635.